Accepted Manuscript

Please cite this article as: Mohammad Hazhir Mozaffari, Majid Ebnali-Heidari, Gholamreza Abaeiani, Mohammad Kazem Moravvej-Farshi, Photonic crystal optofluidic biolaser, Photonics and Nanostructures - Fundamentals and Applicationshttp://dx.doi.org/10.1016/j.photonics.2017.07.002
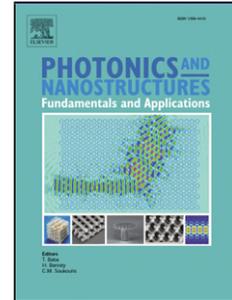
This is a PDF file of an unedited manuscript that has been accepted for publication. As a service to our customers we are providing this early version of the manuscript. The manuscript will undergo copyediting, typesetting, and review of the resulting proof before it is published in its final form. Please note that during the production process errors may be discovered which could affect the content, and all legal disclaimers that apply to the journal pertain.

Photonic crystal optofluidic biolaser

Mohammad Hazhir Mozaffari [a], Majid Ebnali-Heidari[b], Gholamreza Abaeiani[a], Mohammad Kazem Moravvej-Farshi [c, *]

[a] Department of Electrical Engineering, Science and Research Branch, Islamic Azad University, Tehran 1477893855, Iran

[b] Faculty of Engineering, Shahrekord University, Shahrekord 88186-34141, Iran

[c] Faculty of Electrical and Computer Engineering, Advanced Devices Simulation Lab, P.O. Box 14115-194, Tarbiat Modares University, Tehran 1411713116, Iran

GRAPHICAL ABSTRACT
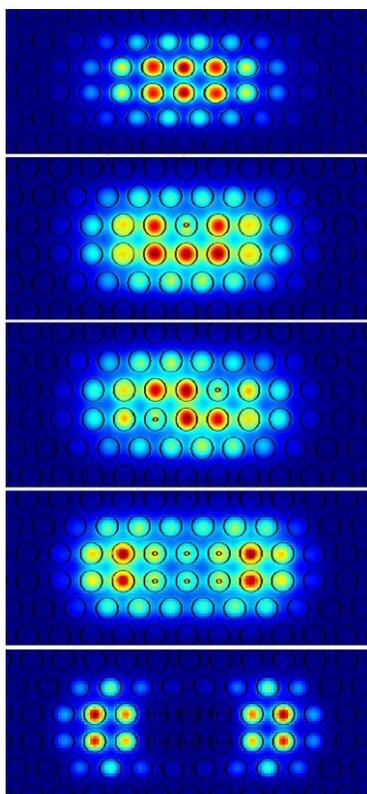
Highlights

- A new optofluidic biolaser based upon the photonic crystal slab with selectively dye-infiltrated air holes is proposed.
- The proposed lab-on-a-chip biolaser is highly sensitive to the minute biological changes that may occur in its cavity.
- This microstructure biolaser can detect a single virus with a radius as small as 13 nm.
- Satisfactory lasing characteristics with power conversion efficiency of 25% and the spectral linewidth of 0.24 nm are achieved.

* Corresponding author: moravvej@modares.ac.ir

Abstract

Optofluidic biolasers are recently being considered in bioanalytical applications due to their advantages over the conventional biosensing methods. Exploiting a photonic crystal slab with selectively dye-infiltrated air holes, we propose a new optofluidic heterostructure biolaser, with a power conversion efficiency of 25% and the spectral linewidth of 0.24 nm. Simulations show that in addition to these satisfactory lasing characteristics, the proposed lab-on-a-chip biolaser is highly sensitive to the minute biological changes that may occur in its cavity and can detect a single virus with a radius as small as 13 nm.

Keywords: Biolaser, Biosensing, Lab-on-a-chip, Optofluidic, Photonic crystal

Nanophotonics merged with microfluidics− i.e., optofluidics− offers a new way of implementing miniaturized optoelectronic devices that can be intrinsically adaptive and reconfigurable. Unique properties of liquids, such as the potential of integration in lab-on-a-chip systems and compatibility with microfluidic components make optofluidic systems highly competitive in the development of biophotonics. Moreover, most of the biochemical reactions should be reproduced in a fluid, making optofluidic system substantially advantageous in biological sensing applications. A novel emerging device in this area is the optofluidic biolaser that can measure changes in biological molecules precisely. When biochemical or biological molecules are incorporated into a gain medium a new class of laser known as the optofluidic biolaser can emerge [1]. A number of optofluidic biosensors based on different principles with diverse advantages, drawbacks, sensitivities, and detection limits, are developed in research and commercial products [2-7]. Among passive sensors, those based on photonic crystals (PhCs) [2-4] or ring resonators [7] show satisfactory sensing signal. However, other types of passive biosensors may experience weak sensing signal and broad spectrum [1].

Laser with features such as stimulated emission, coherency, and resonating amplification offers a fascinating solution to overcome this deficiency and improving the sensitivity. In recent years, a number of optofluidic lasers have been proposed. They have been realized with various types of optical cavities, such as distributed feedback (DFB) gratings [8, 9], Fabry-Perot [10, 11] and ring resonators [12, 13]. Some of these optofluidic lasers are used in biomolecular sensing applications. In addition to biosensing, they can facilitate biomolecular analysis. Interaction of light with a biomolecule that is placed inside a cavity is intensified immensely. Through this intensification, the sensing signal resulted from varying the light characteristic in response to the interaction is amplified. Thus, lasers

characteristics such as input power thresholds, output power intensities, and spectra can provide detailed information about the slightest biochemical and biological changes taking place in the cavities [1]. The first optofluidic biolaser for analysis of biomolecular interactions was demonstrated by [14] and diverse modus operandi have been proposed afterward. One of the outlooks for this technology is the PhC based optofluidic biolaser [1] that has gained a lot of attentions as optofluidic biosensors in the past couple of years. These optofluidic biosensors can be advantageously exploited within optofluidic architectures, while they benefit from characteristics like high quality (Q) factor and low cavity mode volumes that make them more sensitive to the environmental changes than other optical microcavities. A straightforward way of PhC sensing is to monitor the transmission property as the cladding refractive index is changed. Alternatively, in the high index PhCs with complete bandgaps, the cavity can be defined, e.g. by removing one or more holes. The transmission spectrum of the cavity is then monitored when sensing the biological molecules. In other words, the presence of molecules inside the cavity can be detected by monitoring a small spectral shift that has been created due to the interaction of light with molecules. In the PhC based optofluidic biolasers monitoring the lasing characteristic, as well as the transmission spectrum, can be advantageous. Specifically, besides the amplification of the sensing signal, the laser has much more output parameters that can be monitored and serve as a measurement signal. Therefore, optofluidic biolasers provide a powerful technology to analyze changes in biomolecules that may otherwise remain indistinguishable with conventional biosensors.

In this paper, we have reaped the benefits from optofluidics and lab-on-a-chip systems for designing a miniaturized microstructure biolaser based on a solution of organic dye molecules in a solvent as the optical gain medium and a 2D PhC cavity in its original form without any defect. Our initial idea for designing this device was to infiltrate the PhC holes by the active medium. Designing the PhC structure in such a way that optical excitation of lasing material is effectuated, was the major challenge to implementing this idea. Meanwhile, the device should have the potential of integration in the lab-on-a-chip bioanalytical systems. The structure of the proposed optofluidic biolaser is schematically shown in Fig. 1. This biolaser consists of a regular 2D PhC structure, composed of a triangular

lattice of constant $a = 410$ nm and air holes of radii $r = 140$ nm devised in a 220-nm thick suspended slab of Al_2O_3, in which the medial row along the Γ-K direction is removed. Its cross-sectional area is 61-period long and 34-period wide (25×14 μm^2). The fabrication processes can be comparable to those reported for the devices presented in [15, 16].

The medial holes of the PhC slab, depicted by dark red circles in the figure, are considered to be infiltrated with the lasing dye solution, comprising Rhodamine 6G dissolved in ethylene glycol. With this approach a double-heterostructure PhC slab is formed insomuch as the effective refractive index of the midsection is greater than those of the sidewards. This configuration provides the possibility of propagating a specific range of wavelengths in the central region that are not allowed to propagate in the adjacent outer regions. Therefore, the slab acting as a Fabry-pérot cavity, allowing the Fabry-pérot-liked modes to resonate in its middle section provided the condition $2k_xL = 2\pi m$ is satisfied, where k_x is the wave vector of the resonance modes, L is the length of the dye-filled region and $m = 1, 2, 3, \ldots$ is an integer. The structure of the laser chip suggests two wavelength-tuning mechanisms. First, the cavity length can easily be reconfigured by changing the number of infiltrated holes along the PhC length. Second, the type of the dye molecules, its solvent and concentration affect the emission wavelength of the lasing dye. Hence, coupling the output light of the active medium to the laser cavity can be adjustable. The designed lab-on-a-chip laser aims at biomolecules characterization. When a biological molecule is incorporated into the active medium through the chip surface, the laser output intensity changes can be readily monitored. Furthermore, the presence of biomolecules inside the cavity affects the lasing characteristics such as the threshold and power conversion efficiency. It is worth noting that due to facile and feasible fluid infiltration of PhC holes [16, 17], fabrication of the proposed device will be straightforward.

The lasing from Rhodamine 6G can be approximated by a four-level system [18]. Using the finite-difference-time-domain (FDTD) computational method [19], we have modeled the laser dynamics of the four-level atomic system. This model that includes the pumping dynamics and the Pauli Exclusion Principle is more functional than the conventional modal expansion of the electromagnetic field used for complex laser geometries constructed on

PhC platforms. The biolaser was considered to be pumped with a TE-polarized 6 ns pulses of 532 nm wavelength. In this regard, we modeled the Q-switched Nd: YAG laser pulses, commonly used for pumping dye lasers in the practical applications. For an efficient pumping, we should enhance the interaction of the pump light with the dye solution in the designed microcavity with a sharp resonant peak at the pump wavelength. Theoretically, the Q-factor of the designed resonant peak is about 6.2×10^5. Calculating the modal distribution, we can show the presence of a bound TE mode with this resonant wavelength inside the cavity. Fig. 2(a) shows the distribution of the optical electrical field intensity for this mode and demonstrates how strongly this mode is localized within the infiltrated holes of the slab. As seen in this figure, the maximum pump intensity is confined within the six innermost holes of the slab. Therefore, the efficiency of the photopumping is enhanced and the lasing action is facilitated in this miniaturized device. A plot of the laser peak output intensity versus the pump intensity is shown in Fig. 2(b). From this plot, the laser threshold intensity of ~300 V/μm and the optical conversion efficiency of 0.25 can be observed. Figure 2(c) depicts the laser spectra for the pump intensity of 1 kV/μm. The lasing peak occurs at the center wavelength of ~565.5 nm with a linewidth of ~0.24 nm. The optical conversion efficiency and the spectrum linewidth of the designed biolaser are ameliorated in comparison with the conventional microcavity fluidic dye lasers [20, 21]. Comparison of this emission spectrum with those of common lasing dyes reveals that use of the proposed heterostructure biolaser has led to a finer emission characteristic and narrower spectrum. It is worth noting that, this narrow spectrum was achieved mainly by the high Q-factor cavity that supports two modes at the pump and lasing wavelengths.

To investigate the ability of the proposed microchip in bioanalysis applications, we simulate the effect of virus-like particles (VLP) on the lasing characteristics. These particles that can deputize for biologically relevant targets are an important class of biomolecular particles that are composed of self-assembled viral proteins. The VLPs hold potential for a variety of applications ranging from synthetic vaccines to protective vectors for delivery of gene and drug therapies [22]. In our simulations, we use the human papilloma virus-like particles (HP-VLPs) that contain intact capsids but no replication machinery and hence are non-infectious and safe to handle and can readily model

the viral pathogens [23]. The shape of an HP-VLP based on the X-ray crystallography model reported by [24] can be approximated by a spherical core-shell, with the core and shell radii of $r_C = 17.5$ and $r_S = 27.5$ nm, respectively [3]. The refractive indices of the outer viral coat and the interior of the VLP are respectively similar to those of the adsorbed protein layers ($n_s = 1.54$) [25] and the buffer ($n_c = 1.32$) [26]. Using the volume-weighted sum of the refractive indices, the effective refractive index of the core-shell is approximated to be $n_{eff} \sim 1.45$ [3]. The effectiveness of effective refractive index model to describe the interaction between light and the HP-VLP have already been experimentally demonstrated [3]. Considering the surface of the six innermost holes of the PhC slab (Fig. 2(a)) as the capturing area of the biolaser, we apply a VLP to each of these six active holes. This can decrease the pump light confinement in the hole. The distribution of the optical electrical field intensity at the pump wavelength within the PhC is illustrated in Fig. 3 for different fashions of applying VLPs to the PhC holes.

As shown in Fig. 3(a), the presence of just one VLP in a single hole leads to lower the optical field intensity in that hole, preventing the permeated dye solution in that hole to lase effectively while the remaining five dye-filled holes have a greater portion of the laser output. The cavity mode profile for the case in which two holes are infiltrated with a VLP is depicted in Fig. 3(b). In this situation, the privation of the pump light intensity in the two holes that contain VLPs is clearly visible, showing, the dye solutions in these two holes also pose poor laser performance while the remaining four dye-filled active holes take part in the lasing action. The cavity mode profile for the case in which each of the six holes is infiltrated with one VLP is illustrated in Fig. 3(c), while Fig. 3(d) depicts the mode profile for the case in which each hole is infiltrated with two VLPs. As seen from Fig. 3(c), the lasing action in all six VLP infiltrated holes are weakened, while Fig. 3(d) shows that the presence of the second VLP in each hole has diminished the lasing action entirely from the infiltrated holes. These results indicate that virus detection and real-time biological interaction measurements are simply attainable by means of this biolaser. To prove this claim, we have simulated the laser spectra for each of the four cases shown in Fig. 3. The numerical results are presented in Fig. 4(a). The solid curve illustrates the case in which no VLPs are present inside the biolaser. The dashes, dashes-dots, and dots represent the laser spectra for the three cases shown in Fig. 3(a), 3(b),

and 3(c) respectively. Comparison of these four curves reveals a 4% decrease in the peak laser intensity when applying just one VLP in a single hole, a 16.6% decrease in the peak intensity for inserting two VLPs each in a single hole, and ~50% decrease in the biolaser peak intensity when inserting a VLP in each of the six holes. The tiny dashes also represent the laser spectra for the case shown in Fig. 3(d) when there are two VLPs in each of the six holes, showing a 74.8 % decrease in laser peak as compared with that of the no VLP case. It is worth noting that there is a compromise between the detection limit and the ability of detection for a high concentration of VLPs in our reconfigurable design. In the proposed design, in fact, we focused on enhancing the detection limit for a single VLP. In order to make this biolaser capable of detecting a higher concentration of VLPs, it must be redesigned. That is, the slab size and PhC holes diameters must be enlarged, as a consequence of which its detection limit will be weakened.

Moreover, the clear red shift exhibited in the biolaser spectra as the number of VLPs is increased is another embossed effect that can be observed from Fig. 4(a). A 0.4 nm red shift in the peak wavelength was calculated for the presence of 12 VLPs (i.e.; 2VLPs/hole). This shift is comparable to what has been reported for the passive PhC biosensors, experiencing a similar red shift when a virus-carrying cavity is placed in the laser light [3]. To determine the effect of virus size on the laser output, we have simulated the response of biolaser output spectrum to single VLPs of different radii, in the range of 20-80 nm, placed in one of the two middle PhC holes, as shown in Fig.3(a). The pentagrams, observed in Fig. 5(a), show the decrease in the biolaser output intensity versus the VLP radius. As expected, the results show that the output intensity decreases with an increasing in the VLP radius. Finally, to verify the ability of our proposed biolaser to act as an optical biosensor, we have also calculated the spectral red shift induced by the presence of a single VLP in one of the six dye-infiltrated air holes positioned at the center of the PhC slab. The pentagrams, observed in Fig. 5(b), represent the red shift experienced by the biolaser output peak versus the VLP radius. As can be observed from the data illustrated in this figure, the presence of a single VLP of radius 20 nm imposes a ~3.4% decrease in the biolaser peak intensity and a 32.6 pm red shift in the corresponding center wavelength. Both of these variations suggest that the proposed PhC biolaser is capable of detecting a single virion

with the radius of 20 nm. Nonetheless, the estimated sensing limit that obtained from the simulation is ~13 nm that shows a relative improvement as compared to those recently reported for the detection of nanoparticles, using PhC and whispering gallery mode resonators [2, 27].

The detailed analysis of the VLP-induced spectral shift reveals a direct relation between the redshift and the change in the refractive index in one of the dye-infiltrated active hole that can be estimated by

$\Delta n = n_D - (n_D v_D + n_{VLP} v_{VLP})/(v_D + v_{VLP})$, where n_D and n_{VLP} represent the dye and VLP refractive indices and v_D and v_{VLP} are the corresponding volumes. In fact, the magnitudes of the spectral shifts that depicted in Fig. 5(b) for different VLP radii are linearly proportional to the calculated values of Δn.

A careful look at the pump field distributions in the six innermost holes, shown in Fig. 2(a), indicates that the two holes in the middle should contribute slightly more to the laser output than the other holes do. To show this, we interrogated the scenarios in which, a single VLP of various radii is placed in one of the four active holes on the sides and calculated the decrease in peak intensity and the spectral red shift. The results are illustrated in Fig. 5. The comparison of open circles and pentagrams show that the decrease in peak intensity of the biolaser for the case in which the VLP of 20 nm radii is located in one of the four side holes (open circle) is ~ 0.3% smaller than that of the case with an identical VLP located in one of the two middle holes (pentagram), as seen in Fig. 5(a). This variation in peak intensity is practically negligible. Nevertheless, the spectral shift is consistent with both cases, as shown in Fig. 5(b).

Finally, we examine the presence of a single VLP in one of the surrounding holes encircling the six innermost holes. Figures 6(a)-6(f) show the distributions of pumps optical electrical field intensity within the laser. As can be observed in this figure, the presence of a VLP in right side holes (Fig. 6(a) and Fig. 6(c)) and left side holes (Fig. (b) and Fig. (d)) both introduce a shift in the distribution of the field intensity (active region) toward the opposite direction while the number of active holes contributes to the lasing spectra remains unchanged. Consequently, the output laser spectrum also remains intact. The two cases are shown in Fig. 6(e) and Fig. 6(f) depict the field distributions for the

case in which a VLP is placed in one of the holes in the top and bottom surrounding circle, respectively. These two distributions reveal that presence of a VLP in either of this two hole can cause a slight decrease in the pumps' intensity within the hole nearest to the VLP infiltrated hole. Providing a more accurate description, we compare the laser spectrum for these scenarios with the spectrum for the case with no VLP. The comparison is illustrated in Fig. 6(g), indicating little difference in the laser spectra.

In conclusion, we have demonstrated a lab-on-a-chip PhC based biolaser, exploiting a PhC slab with selectively dye-infiltrated air holes but no defects. In the proposed configuration, the slab six innermost holes infiltrated with the dye solution act as the laser gain region. These microdroplets gain medium, are excited optically with a TE polarized light which resonates in the cavity with very high Q-factor. Due to this efficient photo pumping procedure, liquid dyes act as laser and emit light at longer wavelengths than what the pump light is, and likewise, designed microcavity has another resonance peak at the lasing wavelength, leading to narrow output spectra. The fluidic gain medium and the lab-on-a-chip structure of such miniaturized biolaser provide a facility for incorporation of the biological molecules in the gain medium. Furthermore, satisfactory lasing characteristics with power conversion efficiency of 25% and the spectral linewidth of 0.24 nm are achieved. Moreover, simulations that accomplished to ascertain biolaser capability in bioanalytical systems show the ultra-high sensitivity of the device to the biological minute changes occurring in the cavity. As a result, a sole virus with a radius as small as 13 nm would be detectable by means of this optofluidic device. It is worth noting that a significant advantage of this design is its reconfigurability. For bioanalysis applications with a larger number of analytes, requiring a larger area, the chip structure can be redesigned and the cavity length can be expanded conveniently via increasing the number of infiltrated holes.

Simulations, in general, use the effective refractive index model to evaluate the interaction between light and bio-analytes. This model can't, in fact, describe the selective absorption effects of bio-receptors. Due to this limitation, the related model has no ability to differentiate between two different biomolecules with similar shapes and refractive indices. Nevertheless, in practical applications, the biolasers are equipped with bio-

receptors or bio-recognition molecules which enable them to differentiate between target and non-target biomolecules in a body sample. In other words, specificity of a biosensor without using bio-recognition and bioreceptor molecules could not be defined and investigated. Therefore, we couldn't examine any clear approach for sensor specificity in our simulations. Besides the practical approach for capturing the HP-VLPs in photonic crystal structure and its related functionalization process which reported in [3], due to fluidic gain medium, most types of bio-recognition molecules or biomolecules in body fluid samples can readily be attached to the proposed lab-on-a-chip structure. Additionally, ethylene glycol allows attaching all types of alcohol-fast biological particles to the active region of biolaser directly.

References

[1] X. Fan, S.-H. Yun, The potential of optofluidic biolasers, Nat. Methods., 11 (2014) 141-147.

[2] C. Wang, Q. Quan, S. Kita, Y. Li, M. Lončˇar, Single-nanoparticle detection with slot-mode photonic crystal cavities, Appl. Phys. Lett., 106 (2015) 261105.

[3] S. Pal, A.R.Yadav, M.A. Lifson, J. E.Baker, P. M.Fauchet, B. L.Miller, Selective virus detection in complex sample matrices with photonic crystal optical cavities, Biosens. Bioelectron, 44 (2013) 229-234.

[4] S. Arafa, M. Bouchemat, T. Bouchemat, A. Benmerkhi, A. Hocini, Infiltrated photonic crystal cavity as a highly sensitive platform for glucose concentration detection, Opt. Commun, 384 (2017) 93-100.

[5] Edward P. Furlani, R. Biswas, A.N. Cartwright, N.M. Litchinitser, Antiresonant guiding optofluidic biosensor, Opt. Commun, 284 (2011) 4094-4098.

[6] J. Wang, Z. Yao, A.W. Poon, Integrated optofluidic label-free biosensors using a silicon-nitride-based coupled-resonator optical waveguide, 2016, pp. 975014-975014-975010.

[7] M. Li, X. Wu, L. Liu, X. Fan, L. Xu, Self-Referencing Optofluidic Ring Resonator Sensor for Highly Sensitive Biomolecular Detection, Analytical Chemistry, 85 (2013) 9328-9332.

[8] C. Vannahme, M.B. Christiansen, T.Mappes, a.A. Kristensen, Optofluidic dye laser in a foil, Opt. Express 18 (2010) 9280-9285.

[9] M. Karl, G.L. Whitworth, M. Schubert, C.P. Dietrich, I.D.W. Samuel, G.A. Turnbull, a.M.C. Gather, Optofluidic distributed feedback lasers with evanescent pumping: reduced threshold and angular dispersion analysis, Appl. Phys. Lett., 108 (2016) 261101.

[10] L.Yuan, J.Huang, X. Lan, H. Wang, L. Jiang, a.H. Xiao, All-in-fiber optofluidic sensor fabricated by femtosecond laser assisted chemical etching, Opt. Lett, 39 (2014) 2358-2361.

[11] F. Simoni, S. Bonfadini, P. Spegni, S.L. Turco, D.E. Lucchetta, a.L. Criante, Low threshold Fabry-Perot optofluidic resonator fabricated by femtosecond laser micromachining, Opt. Express, 24 (2016) 17416-17423.

[12] S.I. Shopova, J.M. Cupps, P. Zhang, E.P. Henderson, S. Lacey, a.X. Fan, Opto-fluidic ring resonator lasers based on highly efficient resonant energy transfer, Opt. Express, 15 (2007) 12735-12742.

[13] Y. Sun, J.D. Suter, a.X. Fan, Robust integrated optofluidic-ring-resonator dye lasers, Opt. Lett, 34 (2009) 1042-1044.

[14] Y.Sun, X.Fun, Distinguishing DNA by analog-to-digital-like conversion by using optofluidic lasers, Angew. Chem. Int. Ed. Engl, 51 (2012) 1236–1239.

[15] J. Li, T.P. White, L. O'Faolain, A. Gomez-Iglesias, T.F. Krauss, Systematic design of flat band slow light in photonic crystal waveguides, Optics Express, 16 (2008) 6227-6232.

[16] C. L. C. Smith, U. Bog, S. Tomljenovic-Hanic, M. W.Lee, D. K. C. Wu, L. O'Faolain, C. Monat, C. Grillet, T.F. Krauss, C. Karnutsch, R. C. McPhedran, B. J.Eggleton, Reconfigurable microfluidic photonic crystal slab cavities, Opt. Express, 16 (2008) 15887-15896.

[17] A.C. Bedoya, P. Domachuk, C. Grillet, C. Monat, E.C. Mägi, E. Li, B.J. Eggleton, Reconfigurable photonic crystal waveguides created by selective liquid infiltration, Opt. Express, 20 (2012) 11046-11056.

[18] J.T. Verdeyen, Laser Electronics, 3rd Edition ed., Prentice Hall2000.

[19] S.-H. Chang, A. Taflove, Finite-difference time-domain model of lasing action in a four-level two-electron atomic system, Opt. Express, 12 (2004) 3827-3833.

[20] B. Helbo, A. Kristensen, A. Menon, A micro-cavity fluidic dye laser, J. Micromech. Microeng, 13 (2003) 307.

[21] H. Zhou, G.g. Feng, K. Yao, C. Yang, J. Yi, a.S. Zhou, Fiber-based tunable microcavity fluidic dye laser, Opt. Lett, 38 (2013) 3607.

[22] L.F.P. III, D.I. Lipin, D.-H. Tsai, M.R. Zachariah, L.H.L. Lua, M.J. Tarlov, A.P.J. Middelberg, Quantitative Characterization of Virus-like Particles by Asymmetrical Flow Field Flow Fractionation, Electrospray Differential Mobility Analysis, and Transmission Electron Microscopy, Biotechnol. Bioeng., 102 (2009) 845-855.

[23] M.J. Serpe, Y. Kang, Q.M. Zhang, Photonic Materials for Sensing, Biosensing and Display Devices, 1 ed., Springer International Publishing2016.

[24] C.R. Mace, R.C. Rose, B.L. Miller, Tracking serum antibody response to viral antigens with arrayed imaging reflectometry, 2009, pp. 71670H-71670H-71678.

[25] K.L. Prime, G.M. Whitesides, Self-assembled organic monolayers: model systems for studying adsorption of proteins at surfaces, Science, 252 (1991) 1164.

[26] A.H. Harvey, J.S. Gallagher, J.M.H.L. Sengers, Revised Formulation for the Refractive Index of Water and Steam as a Function of Wavelength, Temperature and Density, Journal of Physical and Chemical Reference Data, 27 (1998) 761-774.

[27] L.Shao, X.-F. Jiang, X.-C. Yu, B.-B. Li, W.R. Clements, F. Vollmer, W.Wang, Y.-F. Xiao, Q. Gong, Detection of Single Nanoparticles and Lentiviruses Using Microcavity Resonance Broadening, Adv. Mater, 25 (2013) 5616-5620.
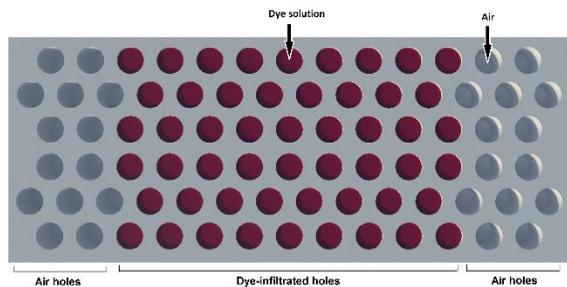
Fig. 1. Schematic top view of the proposed biolaser.
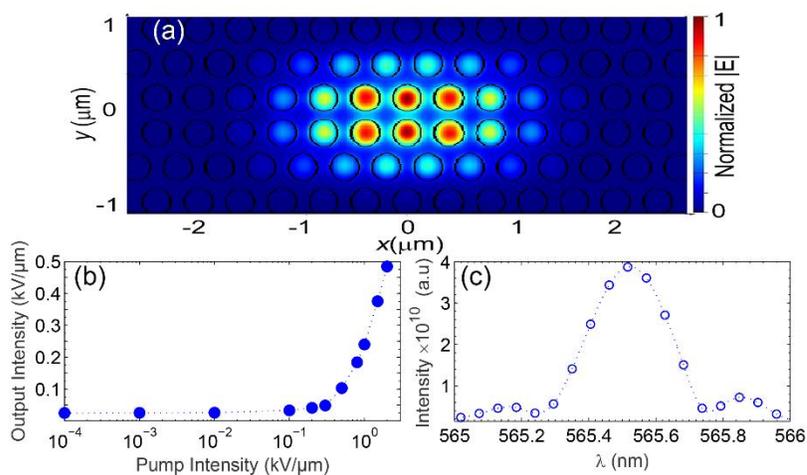
Fig. 2. Distribution of the (a) optical electrical field intensity inside the laser chip at the pump wavelength, (b) peak laser output intensity versus the pump intensity; and (c) lasing spectra at the pump intensity of 1 kV/µm.
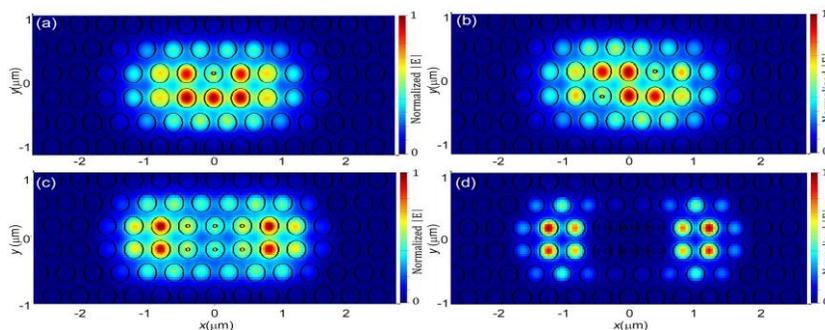
Fig. 3. Distribution of optical electrical field intensity inside the laser chip at pump wavelength for the presence of (a) 1 VLP, (b) 2 VLPs, (c) 1 VLP per each of the 6 innermost holes, (d) 2 VLPs per each of the 6 innermost holes.
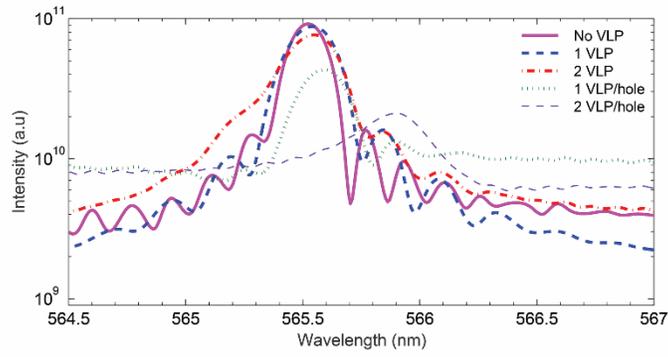
Fig. 4. Lasing spectra of biolaser for several cases of applying VLPs to the gain medium.
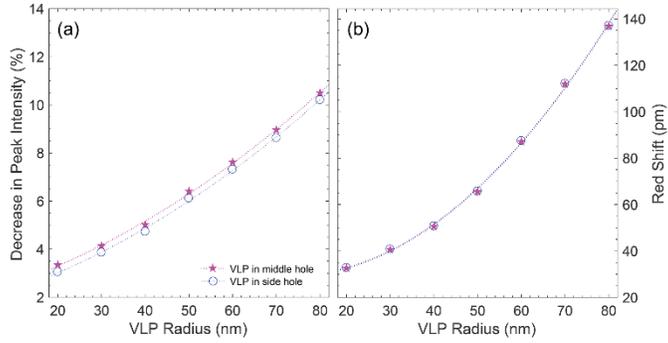
Fig. 5. Effect of VLP radius and location on the (a) biolaser peak intensity decrease and (b) red shift.
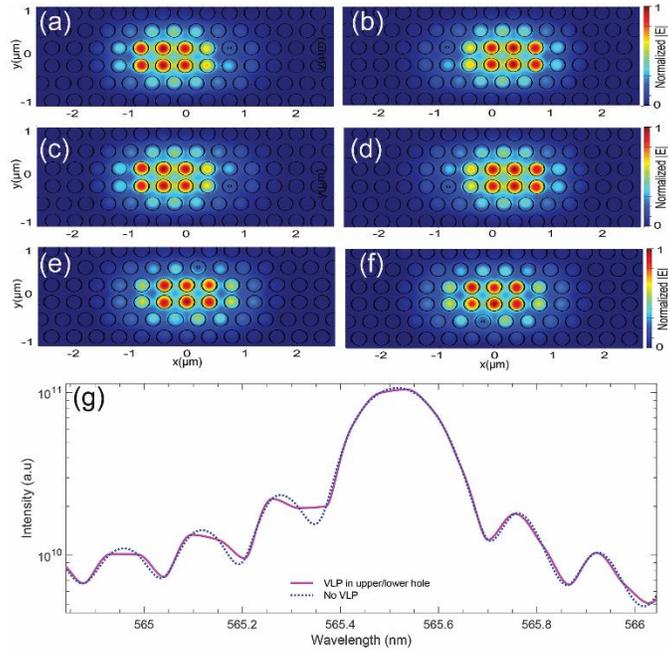
Fig. 6 (a-f) Distribution of pumps' optical electrical field intensity inside the laser chip the presence of a VLP in one of the surrounding holes encircling the six innermost holes. (g) comparison of biolaser spectra for the presence of a VLP in the upper/lower hole of six innermost holes with those for no VLP inside the holes

12